ROMANIAN ACADEMY

Institute of Physical Chemistry „Ilie Murgulescu”

Abstract of the PhD thesis

Study of the electrochemical and electrocatalytic features of some multicomponent materials micro and nanostructured

Scientific advisor:

Dr. Nicolae Spătaru

PhD candidate:

Radu Mihai Marian

Bucharest

2022

Table of contents of the thesis

Keywords

Electrocatalysis; hybrid materials; methanol anodic oxidation; electrocatalysts support materials

Introduction

The PhD thesis titled ***Study of the electrochemical and electrocatalytic features of some multicomponent materials micro and nanostructured*** aimed at contributing to a certain extent to a research topic that attracted electrochemists interest, namely that concerning fuel cells.

This concept is considered of strict actuality because it could help at alleviating nowadays problems related to environmental pollution and fossil fuel shortage, which are issues that all research projects with some "ecological" components seek to solve, at least in part.

In this context, the main objectives of the present work consisted in obtaining new platinum-based electrocatalytic systems (by electrochemical deposition of the noble metal on various micro and nanostructured support materials) and in investigating their performances for methanol anodic oxidation. Attention was also given to the effect of the nature of the substrate on the overall electrocatalytic activity and to the extent of which the investigated systems could represent a viable alternative to traditional Pt/C electrocatalysts currently used for methanol fuel cells applications.

The thesis is structured in five chapters. In the first two chapters, the literature data used to support the own experiments are presented, and in the following three ones, the results of these experiments that aimed to study the electrochemical properties of some new hybrid materials (which we consider relevant for methanol fuel cells applications) as well as their electrocatalytic activity.

Chapter III Electrochemical behavior of silica nanotubes thermally treated in a hydrogen atmosphere and their use as electrocatalysts support [94]

One of the fastest-growing areas of research and technology appears to be the one dedicated to nano-structured materials, primarily because of its huge number of potential applications in numerous fields, such as nanomedicine, biosensors, nanoelectronics and solar energy conversion.[95]

Nano-sized silicon dioxide is among the most popular such materials as it is affordable, highly stable, and can be obtained in various structures with different morphologies and distinct properties.[96] Nevertheless, extensive use of conventional silica as electrode material is somewhat hampered by the lack of intrinsic electron conductivity of the SiO_2 network, although several ways to alleviate this drawback were devised, including the dispersion in the silica bulk of metal nanoparticles[97] or the insertion of conductive polymers.[98]

In this context, special attention was given to ceramic-carbon electrodes which are generally obtained by embedding into the SiO_2 matrix different types of carbonaceous structures such as carbon nanotubes,[99,100] and graphenes,[101] or conductive diamond powder.[102] These composite materials are relatively easily obtained by sol-gel procedures and, at least in principle, well suited for electrochemical applications due to their wide potential window, tunable polarity and high stability.[103]

For the present study, the use of a boron-doped diamond (BDD) substrate appears to be particularly germane because it is reasonable to assume that combining two highly stable materials such as diamond and silica would allow obtaining new types of robust electrode materials.

III.1 Preparation of SiO_2–NT/BDD working electrodes

The synthesis of SiO_2 nanotubes was carried out according to a modified sol-gel method.[109]. Briefly, gaseous ammonia was bubbled for 10 min, at room temperature, through a solution containing tartaric acid, ultrapure water and ethanol and then tetraorthosilicate was added dropwise to the gently stirred solution cooled at 0°C. The gel thus obtained was allowed to stay for 5 h for aging and then filtered. Typically, calcined silica nanotubes (SiO_2-NT) were obtained, after drying the gel for one hour at 100 °C, by thermally treating the silica mass for 3 h, at 500 °C, in air. After that, some calcined silica nanotubes were further annealed (for 1 h at 500 °C) in a hydrogen atmosphere (SiO_2-NT-H) and also used for comparison.

III.2 SEM morphological measurements

The morphology of the calcined silica was scrutinized by scanning electron microscopy and Fig. III.1 shows a typical SEM micrograph. It appeared that SiO_2 hollow structures with tubular shape prevail, although fragments of SiO_2-NT are also incorporated into the bulk of the material. The external diameter of the nanotubes ranges from ca. 300 nm to ca. 3 μm, while their wall thickness fluctuates within the range 100–200 nm. The length of the nanotubes may reach more than 100 μm, and their external surface is well-decorated with spherical SiO_2 nanoparticles.[109]

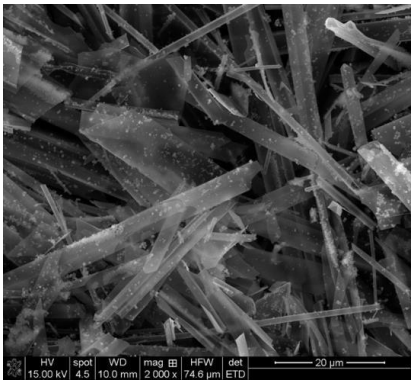

Fig. III.1 SEM micrograph of calcined SiO_2 nanotubes.

The literature dealing with electrochemical applications of undoped silica as such is rather scarce and, to the best of our knowledge, there is no detailed study concerning calcined SiO_2 nanotubes electrochemical behavior. Nevertheless, attention has been given to a certain extent to various $Ru(bpy)_3^{2+}$–SiO_2 nanoparticles systems as possible candidates for cost-effective, regenerable chemical sensors.[116-118]

III.3 Assesement of the electrochemical activity of SiO_2 nanotubes.

To assess the electrochemical activity, cyclic voltammetry experiments were performed and, as curve 2 in Fig. III.2 shows, it was observed, somewhat unexpectedly, that under these experimental conditions the voltammetric response exhibits a very distinct pair of peaks characteristic to $Ru(bpy)_3^{2+}$ presence. The simplest explanation for this behavior would be provided by assuming that SiO_2-NT deposition results in an incomplete coverage of the BDD surface and the redox process can still occur (although more sluggishly) on oxide-free zones of the substrate. However, such hypothesis is ruled out by the fact that, as illustrated by the inset in Fig. III.2, the same electrodes were found to be inactive when $Ru(bpy)_3^{2+}$ species were replaced by the $Fe(CN)_6^{3-/4-}$ redox couple (curve 2 from the inset). These results indicated that SiO_2-NT possesses quite suitable surface structure, chemical composition and electronic properties to enable electrochemical activity for positively charged $Ru(bpy)_3^{2+}$ complex ions.

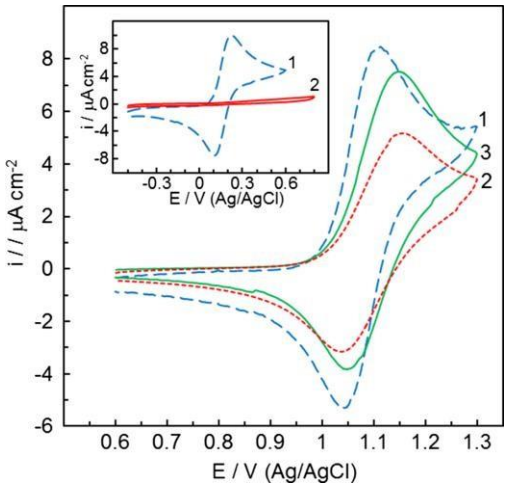

Fig. III.2 Voltammetric responses in 0.2 M KCl + 0.1 mM $Ru(bpy)_3Cl_2$ solution (sweep rate 20 mV/s) recorded at BDD (1), SiO_2-NT/BDD (2) and SiO_2-NT-H/BDD (3). Inset: cyclic voltammograms in 0.2 M KCl + 0.12 mM $K_4Fe(CN)_6$ solution for BDD (1) and SiO_2-NT/BDD (2).

Conversely, as the inset in Fig. III.2 demonstrates, redox processes that involve $Fe(CN)_6^{3-/4-}$ couple cannot occur at the modified electrodes. Such behavior could be understood by taking into account the fact that SiO_2 surfaces are typically negatively charged, due to the presence of hydroxyl and $Si\text{-}O^-$ groups,[119] that might act as strongly repulsive sites for $Fe(CN)_6^{4-}$ ions, thus blocking their access to the electrode surface. One can conclude that the SiO_2-NT coating is responsible for this electrochemical behavior.

This assumption is strongly supported by the observation that the thermal

treatment required for obtaining SiO_2-NT results in the formation of a non-negligible amount of Si^{3+} surface species, besides the prevailing Si^{4+} ones.[115] Si^{3+} sites could be reasonably regarded as negative defects since they represent in fact Si^{4+} species on which one electron is located. The emergence of these negative defects will obviously perturb local charge balance and, for the constraint of global electroneutrality to be met, this process must be necessarily accompanied by the formation of positive defects as well.

With these in mind, a strategy well suited to highlight the role of surface defects should involve purposeful modification of their concentration, followed by the investigation of its effect on the electrochemical behavior of SiO_2-NT. Ostensibly, the most straightforward way to alter the concentration of surface defects (and possibly their nature) would be a further controlled atmosphere annealing, [115,126,127] Furthermore, it was demonstrated that the impregnated H_2 molecules suppress the creation of dangling bonds, but at a price of much enhanced generation of oxygen vacancies.[130]

III.4. Electrochemical impedance spectroscopy measurements

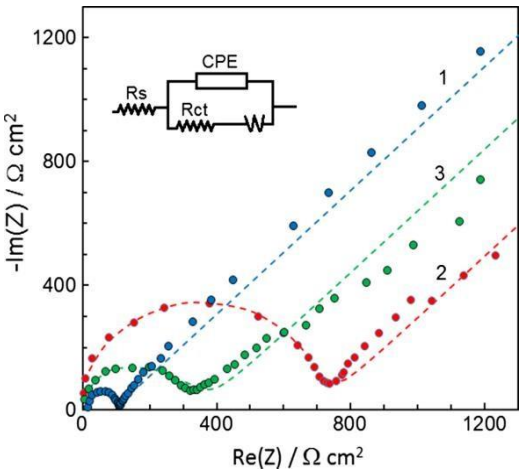

Fig. III.5 Nyquist plots obtained in 0.2 M KCl + 0.25 mM $Ru(bpy)_3Cl_2$ solution for BDD (1), SiO_2-NT/BDD (2) and SiO_2-NT-H/BDD (3) electrodes. Applied potential: (1) 1.07 V; (2,3) 1.10 V. Inset: Electrical equivalent circuit used to simulate impedance spectra.

To better put into perspective this feature, EIS measurements were also performed in a 0.2 M KCl + 0.25 mM $Ru(bpy)_3Cl_2$ solution (at applied potentials corresponding to half-peak potential values estimated from the cyclic voltammograms) and Fig. III.5 shows typical Nyquist plots obtained for bare BDD (curve 1) and for electrodes with similar loadings of SiO_2-NT and SiO_2-NT-H (curves 2 and 3, respectively). The impedance spectra were adequately fitted by using a Randles equivalent circuit (see the inset in Fig. III.5) in which the double layer capacitance was replaced by a constant phase element, in order to account for the roughness of the surface and for its possible physical nonuniformity. It was thus found that subsequent annealing in hydrogen atmosphere of calcined SiO_2 nanotubes undoubtedly promotes $Ru(bpy)_3^{2+}$ anodic oxidation at their surface, as clearly demonstrated by the decrease of the charge transfer resistance from ca. 706 Ω cm^2 at SiO_2-NT/BDD to ca. 364 Ω cm^2 at SiO_2-NT-H/BDD. As anticipated from the cyclic voltammetry results, the same process takes place more easily at bare BDD, which is reflected in a much lower value of the charge transfer resistance (ca. 93 Ω cm^2).

III.5 Influence of the thermal treatment in hydrogen atmosphere

In order to get more insight into the way in which the hydrogen thermal treatment influences the electrochemical activity toward redox processes involving $Ru(bpy)_3^{2+/3+}$ species, cyclic voltammograms recorded at both SiO_2-NT/BDD and SiO_2-NT-H/BDD electrodes were fitted by means of a DigiSim 3.03 (Bioanalytical Systems, Inc.) software.

To better put into evidence this behavior the cathodic charges corresponding to experimental and simulated cyclic voltammograms were compared, for both types of SiO_2 nanotubes, on a relative basis. For SiO_2-NT the experimental value (31.8 μC cm^{-2}) was in excellent agreement with the calculated one (31.4 μC cm^{-2}), whereas in the case of SiO_2-NT-H the simulation yielded a charge of 41.4 μC cm^{-2}, with ca. 37% higher than the experimental value (30.1 μC cm^{-2}). This is an indication of the fact that although hydrogen annealing results in an increase of the number of sites which are active for the anodic process, this treatment does not necessary lead to a similar increase of the number of sites prone to give off electrons during the reverse cathodic scan. Such behavior is somewhat intriguing since the electric charge corresponding to positive defects (possible electron acceptors) should balance that of the negative ones (possible electron donors) and it would be expected that an increased number of the latter (evidenced in the XPS spectra by the higher surface concentration of Si^{3+} species) would proportionately enhance the cathodic current.

III.6 Methanol anodic oxidation on Pt-modified SiO_2–NT–H nanotubes

In order to gauge the activity of the platinum electrocatalyst, methanol anodic oxidation was chosen as a test-reaction and the shape of the recorded cyclic voltammograms were characteristic of methanol oxidation at platinum electrodes, as they exhibited two anodic peaks: the first one on the forward scan at ca. 0.8 V, and a second one, located at ca. 0.6 V, on the reverse, cathodic, scan.

To place these results in a more practical context, Pt/ SiO_2-NT-H/BDD electrodes were also used for steady-state polarization experiments, carried out by increasing the applied potential in 10 mV steps and allowing 10 min after each step for the stabilization of the current. Lower potential values are of particular interest for applications, and it was observed that for an applied potential lower than ca. 0.5 V the fitted Tafel slope is of ca. 116 mV/decade indicating that the rate-determining step involves methanol molecules dehydrogenation.[138] At higher potentials, the Tafel slope increases significantly (up to ca. 220 mV/decade), this behavior being usually attributed to the fact that the rate-determining step shifts to the oxidation of CO like adsorbed species.[139] Such values of the Tafel slope are encouraging as they compare reasonably well with those of 115–289 mV/decade reported for conventional PtRu catalysts.[140-142]

CHAPTER IV – Improvement of the electrocatalytic performances of Pt/TiO_2 systems by laser treatment of the oxide support[146]

IV.1 Introduction. Potential advantages of the TiO_2 support

Starting from the pioneering works in the early 1950s,[147] the concept of methanol fuel cells continued to attract a steadily growing interest, mainly because such systems were considered to be a viable alternative for high efficiency energy conversion. Furthermore, it was deemed that their application on a larger scale might help in alleviating to some extent foreseeable problems related to environmental pollution and fossil fuel shortage. At present, methanol fuel cells require very costly Pt electrocatalysts,[148] and although numerous research groups went to great lengths in the effort of finding active, precious metal free, electrocatalysts, at this stage, the extent to which this demand will be met depends on the successfulness of the attempts to minimize the platinum content while maintaining high activity of such electrocatalysts.[149]

A propitious way to avoid these problems was found to be the deposition of platinum or platinum alloys on a titania substrate, as this enables uniform dispersion of the electrocatalyst nanoparticles.[161] More importantly, it was demonstrated that, when supported on TiO_2 substrates, Pt-based catalysts exhibit enhanced activity for methanol anodic oxidation, due to strong metal-support interactions, to the partial reactivation of active sites by hydrogen spillover, and to the fact that the titania surface includes –OH groups that can act as oxygen donors, facilitating further oxidation of CO adsorbed species. It is also worthy of note that titania subtrates can also lend a hand in enhancing methanol oxidation on Pt-based electrocatalysts by photo-assistance.

Undoubtedly, one of the most remarkable asset of titanium lies in the fact that its exposure to air or to solutions leads, within nanoseconds, to spontaneous surface passivation, due to the formation of a very thin (4–6 nm) protective layer consisting of low-crystalline or amorphous TiO_2.[190,191] More recent studies have demonstrated that, since they are thin enough to allow electron tunneling, such, very stable, native air-formed titania films may be successfully used as platinum supports for oxygen reduction reaction.[192]

IV.2 Treatment of TiO_2 films and Pt/TiO_2 obtaining

In order to enable the formation of uniform, high surface area, oxide films, the titanium substrate was subjected to an etching procedure commonly used in the literature,[193-195] which ensures an appropriate degree of roughness of the metal surface. Subsequently, some of the samples were micromachined by means of a laser engraving setup and the working conditions were appropriately adjusted in order to avoid significant oxidation of titanium substrate.[187]

Platinum particles were deposited electrochemically from a 0.1 M KNO_3 + 0.01 M $HClO_4$ + 4.5 mM H_2PtCl_6,, by applying consecutive potentiostatic pulses (applied potential, –0.15 V) of 5 s each, both on the native air-formed titania films (N–TiO_2) and on the laser-treated ones (LT-TiO_2). Electrochemical measurements were performed with a PAR 273A potentiostat, in a three-electrode glass cell by using a Ag/AgCl

electrode (in saturated KCl) as reference and a platinum gauze as counter electrode.

IV.3 Laser-modification of morphological and textural features of titanium oxide surface

SEM micrographs from Fig. IV.1 clearly illustrate the modifications of the morphological and textural features of the titanium oxide surface, induced by the laser treatment. As Fig. IV.1b shows, the treatment results in the occurrence of two orthogonal grids of mutually perpendicular lines, with regular spacing. Both sets of lines can be more distinctly identified in Z-contrast images (see the inset in Fig. IV.1b), which would indicate the presence of oxygen enriched zones.[196] At the microscale, it appears that faceted grains with sharp edges and irregular zones (typical of a chemically etched surface) observed before treatment (Fig. IV.1c) change into rounded surfaces, indicating a melt solidification process (Fig. IV.1d). More importantly, it was observed that, at nanoscale, the laser treatment also resulted in a significant change of the morphology, as a clear granularity appears, covering all the surface, with both very fine and homogeneous grains and pores with typical size of a few nanometers (compare insets in Figs. IV.1c and IV.1d).

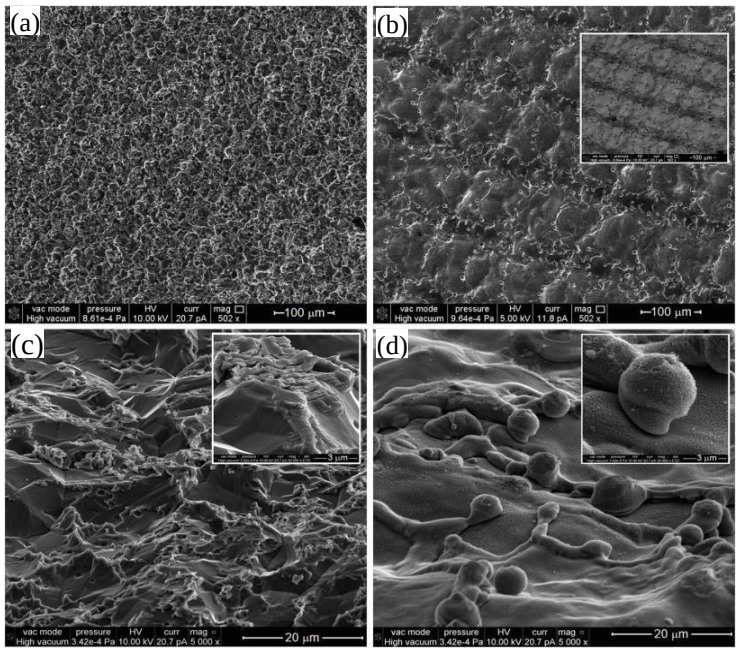

Fig. IV.1 SEM images of native air-formed titania, before (a, c) and after (b, d) the laser treatment. Insets: b) corresponding Z-contrast image; c) and d) corresponding SEM micrographs at higher

IV.4 Effect of the laser treatment on the surface chemical composition

The effect of the laser treatment on the surface chemical composition of the titania-coated samples was also explored by XPS and the results are illustrated by the narrow-scan spectra from Fig. IV.2. It was noticed that before the treatment the deconvoluted Ti 2p spectrum exhibits a very intense doublet (BE 458.7 and 464.4 eV) characteristic to the presence of TiO_2, and two additional ones (BE 454.1 and 460.5 eV and BE 456.3 and 461.7 eV), much smaller, ascribed to metallic titanium and to Ti suboxides.[197] In terms of relative surface concentration, titanium dioxide largely prevails (90.3%) whereas Ti^0 and titanium suboxides concentrations are significantly lower (4.7% and 5.0%, respectively). As Fig. IV.2b shows, at the laser treated surface,

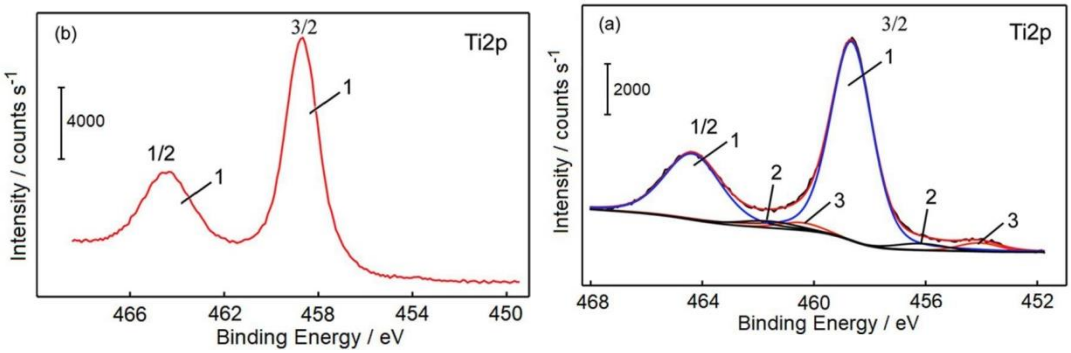

Fig. IV.2 High-resolution XPS spectra recorded Ti 2p region for N–TiO_2 (a) and LT-TiO_2 (b) fitted with Voigt functions assigned to Ti^{4+} (1), titanium suboxides (2) and metallic Ti (3).

XPS measurements evidenced the presence of TiO_2 only. This suggests that the laser-induced melting-solidification process revealed by the SEM measurements is also accompanied by further oxidation of the small amount of titanium species with lower oxidation states.

IV.5 Photoelectrocatalytic activity of titanium oxide films

The photoelectrochemical activity of the native formed titania films (N–TiO_2) and of the laser-treated ones (LT-TiO_2) was checked in a 0.1 M KNO_3 + 0.01 M $HClO_4$ solution, in a potentiodynamic regime (sweep rate, 10 mV mV s^{-1}) and the results obtained for chopped UV-illuminated conditions are shown in Fig. IV.3. As expected for n-type semiconductors, in both cases photoanodic effects were recorded and it appears that the laser treatment led to a significant enhancement of the photocurrent (curve 2 in Fig. IV.3). The inset in Fig. IV.3 shows typical dark current responses recorded both for N–TiO_2 (curve 1) and for LT-TiO_2 (curve 2) and it was noticed that after the laser treatment the capacitive-like background current, within the potential range 0.2–0.4 V, increases with ca. 33%. It is reasonable to ascribe this increase to the corresponding enhancement of the specific surface area of the oxide films, evidenced by the SEM measurements (see the insets in Figs. IV.1c and IV.1d).

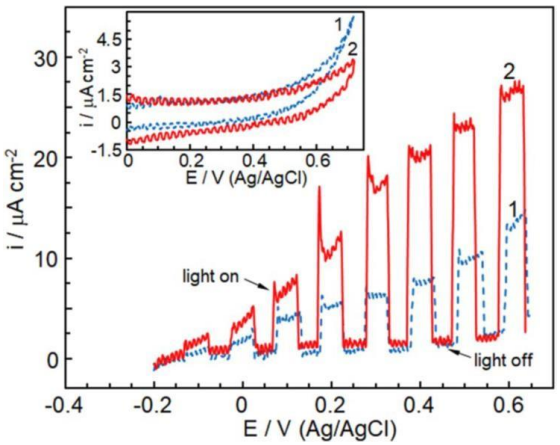

Fig. IV.3. Current-potential dependence (sweep rate of 10 mV/s upon intermittent UV-irradiation recorded in 0.1 M KNO_3 + 0.01 M $HClO_4$ at N–TiO_2 (1) and LT-TiO_2 (2) electrodes. Inset: corresponding cyclic voltammograms recorded in dark

Interestingly, as the results from Fig. IV.3 demonstrate, within the same potential range the photocurrent recorded for LT-TiO_2 is approximately twice that observed for N–TiO_2. This is clear indication of the fact that the enhancement of the photocurrent is not only the result of the higher roughness of the surface but is also due

to some improvement of the charge carrier separation. There are reasons to believe that Ti suboxides species observed in the N–TiO_2 XPS spectra may act as recombination centers, with deleterious effects on the photoactivity.

IV.6 Study of the morphology and surface chemical composition of Pt/N–TiO_2 and Pt/LT–TiO_2 systems

Both N–TiO_2 and LT-TiO_2 structures were further used as substrates for platinum electrochemical deposition, the morphology of the Pt deposits was checked by SEM, and Fig. IV.4 shows typical images obtained for both types of electrodes. It was

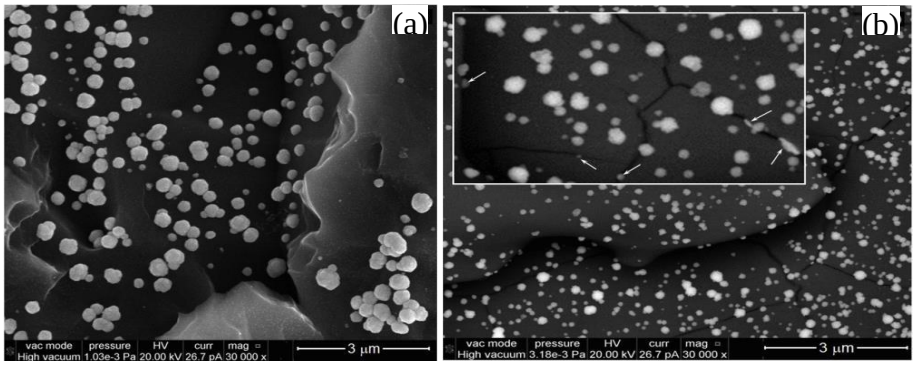

Fig. IV.4 SEM images of the electrodes at Pt/N–TiO_2 (a) and Pt/LT-TiO_2 (b). Pt loadings (μg cm^{-2}): a) 15.7; b) 15.4 Inset: Pt/LT-TiO_2 enlarged image; arrows indicate entrapped Pt particles.

observed that, when deposited on N–TiO_2, most of the particles are of relatively large size (ca. 250 to ca. 400 nm) and tend to agglomerate, leading to clusters formation (Fig. IV.4a). Conversely, as Fig. IV.4b illustrates, the use of a laser-treated substrate enables obtaining not only a more uniform distribution but also a significantly lower average size of the Pt particles (ca. 75 nm). It appeared that the laser-induced melting-solidification process results in the formation of surface micro-cracks (better visible on the inset in Fig. 4b), most likely due to some thermal stress induced by the differences in terms of thermal expansion coefficients between the oxide film and the metallic substrate. Nevertheless, in the context of the present work, this is not a matter of concern since these cracks are only superficial and do not reach the titanium surface, as demonstrated by the LT-TiO_2 XPS spectra (Fig. IV.2b).

A possible explanation for the larger size and the less homogeneous dispersal of the Pt particles on the Pt/N–TiO_2 electrodes surface can be provided by observing that, before the laser treatment, the titania surface exhibits a large number of sharp edges (Fig. IV.1c). During the initial stage of the Pt cathodic deposition the current density on these edges will be higher, which will obviously favor the process. Further deposition will occur mainly on the already deposited platinum rather than on the less conductive titania surface, leading to the formation of larger aggregates. On the contrary, LT-TiO_2 surfaces are free of such problems because, as SEM and XPS measurements revealed, the laser treatment results in a quite levelled titania surface, with a homogeneous chemical composition.

IV.7 Electrochemical activity of TiO_2 electrodes modified with Pt nanoparticles

The electrochemical activity of the Pt-decorated electrodes was firstly checked by cyclic voltammetry (sweep rate, 20 mV/s) in the supporting electrolyte (0.1 M KNO_3 + 0.01 M $HClO_4$) and the inset in Fig. IV.6 shows reproducible voltammetric responses recorded after stabilization for both Pt/N–TiO_2 (curve 1) and Pt/LT-TiO_2 (curve 2) electrodes, the shape of the cyclic voltammograms, being characteristic of Pt behavior in acidic media, It is also worthy of note that, for Pt/LT-TiO_2, the cathodic peak on the reverse scan preceding hydrogen adsorption is anodically shifted with ca. 100 mV, compared to the case of Pt/N–TiO_2 electrodes. This is an indication that, when platinum is deposited on the laser-treated substrate, Pt oxides formed during the direct anodic scan are less stable and will more easily undergo electrochemical reduction.

In order to evaluate the influence of the laser treatment of the TiO_2 substrate on the electrocatalytic effectiveness of the deposited platinum, methanol anodic oxidation was investigated by cyclic voltammetry and Fig. IV.6 displays exemplary responses recorded during the fifth run for both Pt/N–TiO_2 (curve 1) and Pt/LT-TiO_2 (curve 2). It appears that, as expected for methanol oxidation on platinum, at Pt/LT-TiO_2, the voltammograms exhibit two well-defined anodic peaks: a peak on the anodic scan (located at ca.0.55 V) corresponding to methanol oxidation on oxidized platinum and another one, on the reverse scan (peak potential, ca. 0.35 V), usually attributed to the eviction from the Pt surface (more or less oxide-free) of partially oxidized carbonaceous species formed during the anodic scan.[202] For Pt/N–TiO_2 electrodes (curve 1 in Fig. IV.6), the shape of the voltammogram, the higher peak potentials and the rather ill-defined anodic peak on the forward scan (peak potential, ca. 0.74 V) indicate more sluggish kinetics for methanol oxidation. A possible explanation for this behavior lies in the larger average size of the platinum particles, since it was postulated that at oxide-supported platinum, methanol oxidation is significantly promoted on the smaller particles, whereas larger ones are fully active only at higher potentials.[113,203]

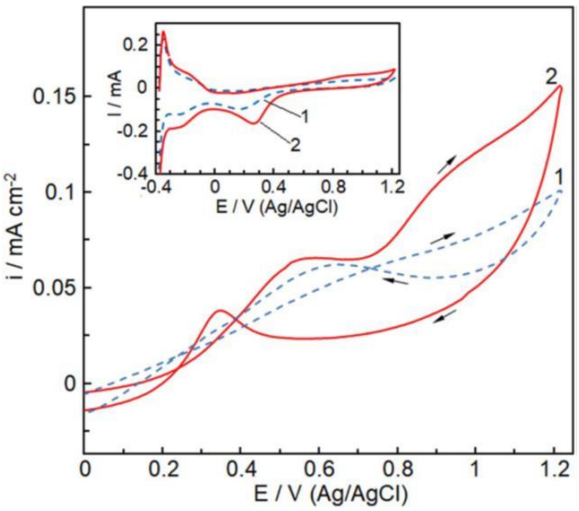

Fig. IV.6 Characteristic cyclic voltammograms recorded at Pt/N–TiO_2 (1) and Pt/LT-TiO_2 (2) electrodes during the fifth cycle in 0.1 M KNO_3 + 0.01 M $HClO_4$+ 2.25 M CH_3OH (sweep rate, 20 mV/s). Inset: corresponding voltammetric responses recorded in the absence of methanol.

It was also found that at potential values higher than ca. 0.8 V (which are, however, of limited interest for practical applications) the voltammograms recorded at Pt/LT-TiO_2 (curve 2 in Fig.IV. 6) exhibited an additional peak around 0.9 V that could be assigned to the oxidation of linear bonded carbon monoxide[204] which takes place during incipient oxygen evolution, leading to CO_2 formation.[205]

A frequently used criterion for the evaluation of the activity for methanol oxidation of platinum-based electrocatalysts is the ratio of the forward peak current density to the reverse peak one (i_f/i_r), the increase of which indicates better resistance to deactivation via strong adsorption of carbonaceous intermediate species. In the present case, as Fig. IV.6 indicates, an i_f/i_r ratio close to 0.8 was found for Pt/N–TiO_2, whereas the use of a laser-treated substrate resulted in a value of ca. 1.5. This is clear proof of a better resistance to fouling during methanol oxidation of the Pt/LT-TiO_2 electrodes.

IV.8 Methanol anodic oxidation at Pt/LT–TiO2, a photo-assisted process

In order to assess the benefits of using laser-treated TiO_2 as platinum support for possible fuel cell applications, chronoamperometric experiments were performed in the presence of 3 M CH_3OH, at an applied potential of 0.5 V. As curves from Fig. IV.7 illustrate, UV irradiation of the Pt/LT-TiO_2 electrode surface results in a strong enhancement of the methanol oxidation current, probably due to the fact that the presence of oxygenated species on the titania surface facilitates desorption of intermediates.[206]

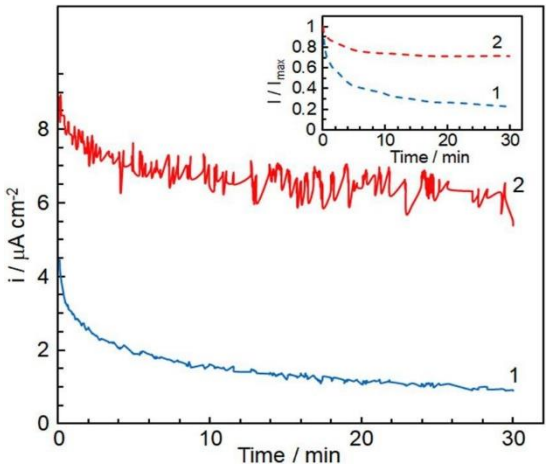

Fig. IV.7 Chronoamperograms for methanol oxidation recorded in 0.1 M KNO_3 + 0.01 M $HClO_4$ + 3.0 M CH_3OH at Pt/LT-TiO_2 electrodes in dark (1) and under UV irradiation (2). Inset: corresponding time dependence of the oxidation current normalized by its maximum value.

To better put these results into perspective, the inset in Fig. IV.7 shows the time dependence of the oxidation current normalized by its maximum value (I/I_{max}). It was found that 30 min of continuous polarization in dark results in the decrease of the current to ca. 20% of its initial value (curve 1 from the inset in Fig. IV.7) whereas, under UV irradiation this decrease is less significant (to ca. 70% only). This lower sensitivity to deactivation can be ascribed not only to a partial regeneration of the electrocatalyst active sites by the bifunctional mechanism, but also to the fact that, as previously demonstrated, UV-light can stimulate carbon monoxide desorption by weakening the Pt–CO chemical bond.[207]

It is important to note that the vast majority of the Pt/TiO_2 systems that are believed to be relevant for fuel cell applications consist of Pt–decorated titania particles, which ensure a high active surface area and are suitable for being used in membrane electrode assemblies. Obtaining such systems usually involves chemical deposition of platinum, which might not always provide very good metal–oxide electrical contact and it seems more advantageous to deposit the platinum electrochemically (as in the present work), thereby ensuring that all the noble metal is in direct electrical contact with the titania substrate, and therefore can, in principle, be electrochemically active.

CHAPTER V – Performances as electrocatalyst support of graphene–conductive diamond powder composites[216]

V.1 Graphene as electrocatalysts support

Successful application of various forms of carbon in numerous electrochemical fields marked an important milestone in the past extensive quest for highly performant electrode materials. In many cases it was found that carbonaceous materials, including graphene, surpass noble metal-based ones, primarily due to their noteworthy advantages, such as good electrocatalytic activity for different redox processes, wide potential window, satisfactory mechanical and electrochemical stability, and, still importantly, cost-effectiveness.[217]

Nevertheless, it was observed quite frequently that, both in terms of surface specific area and electrochemical activity, the performances of graphene-modified electrodes are not as noteworthy as those associated with individual, single-layer, graphene.[228,229] The main reason for this behavior seems to be the fact that such electrodes are usually obtained by simply immobilizing the graphene material on some conductive substrate and, due to van der Waals interactions, graphene sheets tend to agglomerate and can even restack as graphite particles. This aggregation not only results in a smaller active surface area but also leads to a decrease of the density of edge plane sites[229] which are much more active for redox processes than the basal plane ones.[230]

One of the most widely used approaches to alleviate such issues is the use of spacers, which are in fact different types of nanoparticles that are purposefully introduced between the graphene sheets to prevent their aggregation. Apart from these more or less laborious procedures, the simpler approach of drop casting ultrasonicated dispersions of graphene mixed with carbon black or carbon nanotubes also resulted in a significant degree of sheets separation, with beneficial effects on the efficiency of ion transport to the graphene surface.[241,242]

These promising results prompted us to investigate the extent to which conductive boron-doped diamond powder (BDDP) could be used for the same purpose, such approach being legitimized not only by the outstanding features of conductive diamond[243] but also by the successful efforts to obtain BDDP by boron-doping inexpensive, commercially available, diamond particles.[244,245]

V.2 Working electrodes obtaining

For the present work commercially available graphene (GR) nanoplatelets (Goodfellow) was used, while conductive diamond powder (BDDP) was prepared at Tokyo University of Science by using microwave plasma-assisted chemical vapor deposition for growing boron-doped diamond on a natural diamond powder.

A sample of graphene (6 mg) was mixed with 30 μL Nafion solution (5%) and 970 μL isopropyl alcohol, the suspension thus obtained being sonicated for one hour. Similar procedure was followed by using a GR+BDDP mixture (weight ratio, 5:1). To prepare working electrodes, appropriate amounts of the above suspensions were drop-casted on substrates, consisting of highly boron-doped polycrystalline diamond (BDD) films grown on silicon wafers. After drying in air at room temperature, some of the modified electrodes were used as supports for platinum deposition, carried out from a

0.5 M H_2SO_4 + 4.8 mM H_2PtCl_6, solution, by applying consecutive potentiostatic pulses (pulse duration, 5 s, applied potential −0.15 V) and the Pt loading was then calculated based upon the cathodic charge integrated during the deposition.

The electrochemical experiments were performed under deaerated conditions, in a conventional three-electrode glass cell at room temperature, by means of a PAR 273A potentiostat. The counter electrode consisted in a platinum gauze and a Ag/AgCl electrode in saturated KCl solution was used as reference. For the CO stripping measurements the electrolyte solution (0.5 M H_2SO_4) was deaerated with Ar for 30 min, and then CO was bubbled into the solution for 15 min, in order to allow CO adsorption. Before initiating the voltammetric scan, argon was bubbled again for 30 min to remove dissolved CO and during this whole procedure the electrode was kept at an applied potential of –0.25 V.

V.3 Characterization of GR–BDDP composite and of individual components

Raman spectroscopy is one of the most powerful techniques to study the structure of carbon materials and every carbon allotrope can be identified in the Raman spectra (RS) by its specific features. Fig. V.1 presents the spectra of graphene (GR), boron-doped diamond powder (BDDP), BDD film substrate and GR-BDDP.

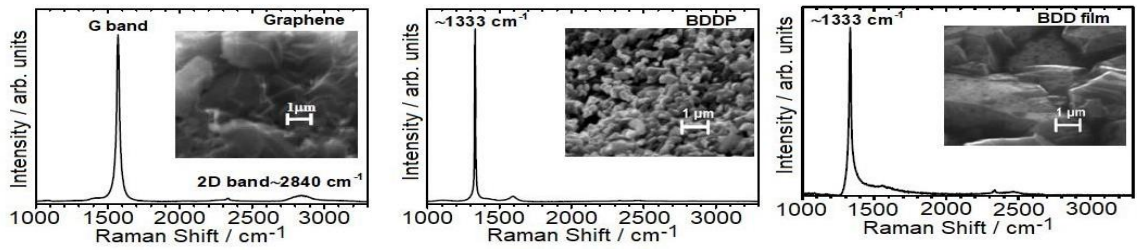

Fig. V.1 Raman spectra and corresponding SEM micrographs of GR (a), BDDP (b), BDD film substrate (c)

V.4 Effect of the boron-doped diamond powder addition

In order to check the effect of the BDDP addition on the surface chemical composition of the graphene-modified electrodes XPS measurements were carried out and Fig. V.3 shows characteristic spectra recorded in the C1s core level region for GR (Fig. V.3a) and GR-BDDP (Fig. V.3b).

In both cases the deconvoluted spectra exhibit four peaks, the major one situated at 284.4 eV being ascribed to the presence of sp^2 carbon from the C─C graphene ring[256,257]. The second peak (285.3 eV) indicates the presence, even in the GR sample, of a certain amount of sp^3 carbon.[258]

Two other peaks are observed in the C1s spectra assigned to carbon singly bounded to oxygen (C–O) and to carboxylate groups (C=O) located at binding energies of 286.3 and 287.6 eV, respectively.[256] In terms of relative surface concentration, sp^2 hybridized carbon species prevail in both cases (78.8% for GR and 77.2% for GR-BDDP) while the addition of the conductive diamond powder leads to a slight increase of the sp^3 carbon surface content (from 10.2% to 14.8%). It was also observed that

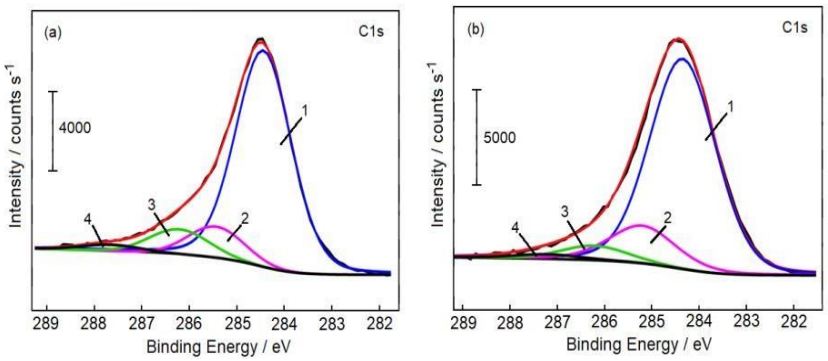

Fig. V.3 Narrow-scan XPS spectra in the C 1 s region recorded for GR (a) and GR-BDDP (b) and fitted by overlapping Gaussian-Lorentzian curves assigned to: sp^2 carbon (1), sp^3 carbon (2), C–O (3) and C=O (4) groups.

BDDP incorporation results in a non-negligible decrease of the oxygenated functional groups surface concentration, from 8.8% to 6.5% for C–O and from 2.2% to 1.5% for C=O.

V.5 Electrochemical activity of the GR–BDDP composite

To straightforwardly assess the effect of the presence of the conductive diamond powder on the electrochemical activity of the graphene- modified electrodes, preliminary cyclic voltammetry experiments were performed and the results obtained with both GR and GR-BDDP were compared on a relative basis. To minimize the effect of the surface chemistry of the carbonaceous electrodes on the electron transfer kinetics, $Ru(NH_3)_6Cl_2$ was used as test-compound since this redox system is known to be a typical outer-sphere one. Characteristic voltammetric responses illustrated in Fig. V.4 show that BDDP addition results not only in a slightly higher peak current but also in a decrease of the anodic–cathodic peak separation (from ca. 274 mV for GR to ca. 80 mV for GR-BDDP).

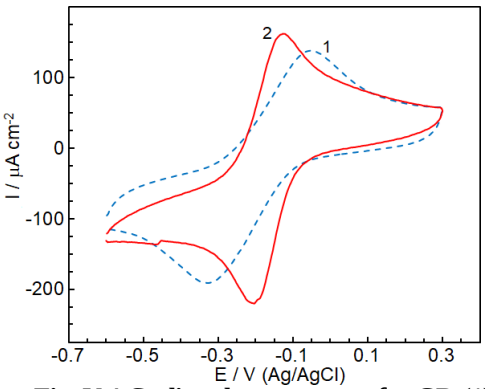

Fig. V.4 Cyclic voltammograms for GR (1) și GR-BDDP (2) in 1 M KCI + 1 mM $Ru(NH_3)_6C1_2$ (sweep rate, 20 mV/s)

To better compare, in terms of morphology, the two types of electrodes a porosity factor can be calculated as $P = k[I_P(500\ mV/s)/I_P\ (5\ mV/s)]$, where $I_P(500\ mV/s)$ and $I_P(5\ mV/s)$ are the anodic peak currents at the corresponding sweep rates, while k stands for the ratio $(5/500)^{1/2}$.[260] Values of P of 1.05 and 1.23 were found for GR and GR-BDDP electrodes respectively, indicating that BDDP addition results in a more loose and, consequently, more porous morphology of the carbonaceous deposit. These findings are also in agreement with the apparent enhancement of the electrocatalytic activity observed for GR-BDDP since it was previously demonstrated that a larger porosity factor corresponds to a smaller peak-to-peak separation.[259]

V.6 Characterization of Pt/GR and Pt/GR–BDDP hybrid systems and their electrocatalytic activity for methanol anodic oxidation

Both GR and GR-BDDP were further used as substrates for platinum electrodeposition and Fig. V.6 shows typical SEM micrographs of the Pt-decorated electrodes thus obtained. It appears that on the graphene support platinum particles are smaller (average size, ca. 250 nm) and somewhat more uniformly distributed (Fig. V.6a) whereas, on the GR-BDDP one, an increase of the agglomeration tendency is observed resulting in a higher average size (ca. 530 nm) of the noble metal particles (Fig. V.6b). It was also interesting to observe that, for Pt/GR-BDDP, the slightly better separation of the graphene platelets promotes to some extent cluster formation on their edges, although small Pt particles are also deposited on the BDDP grains. Due to this feature, the platinum deposit consists mainly of better exposed Pt aggregates, which should be, at least in principle, more accessible to electrochemically active compounds.

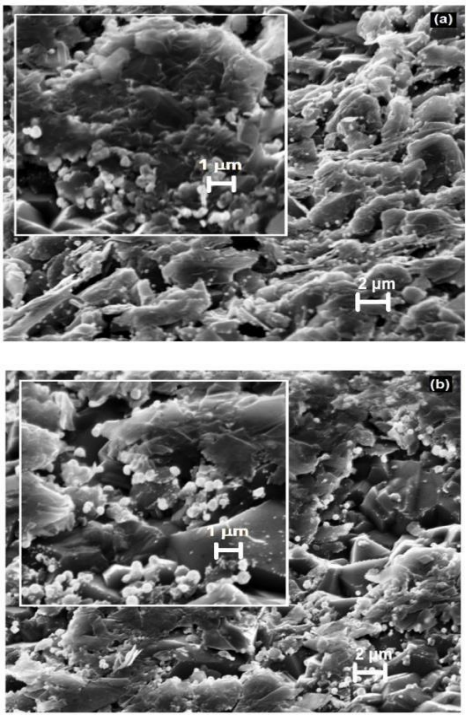

Fig. V.6 SEM micrographs for pentru Pt/GR (a) and Pt/GR-BDDP (b) electrodes

Currently, the extensive research performed on the carbon-supported platinum electrocatalysts is motivated to a great extent by their possible use as active electrode materials for energy conversion systems, among which methanol fuel cells are perhaps the more enticing. Nevertheless, efficient methanol anodic oxidation is frequently hindered by the marked tendency of the platinum to strongly adsorb reaction intermediates (especially CO), leading to the electrocatalyst fouling. These reasons prompted us to investigate the anodic oxidation of irreversibly adsorbed carbon monoxide, in the absence of dissolved CO, and Fig. V.8 shows stripping voltammograms (corrected for the background current) recorded for both Pt/GR (curves 1a and 1b) and Pt/GR-BDDP (curve 2).

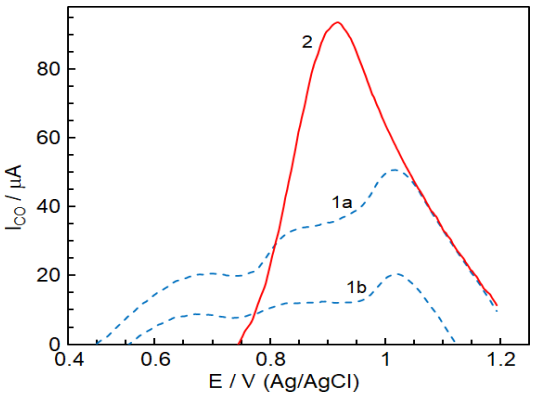

Fig. V.8 Stripping voltammograms of adsorbed CO recorded in 0.5 M H_2SO_4 at Pt/GR (1) during the first run (a) and the second consecutive one (b) and at Pt/GR-BDDP (2). Sweep rate, 20 mV/s.

It was observed, somewhat surprisingly, that in the case of Pt/GR electrodes carbon monoxide is not completely stripped-out during the first run (curve 1a) and its oxidation continues even throughout the second, consecutive one (curve 1b), which involves ca. 24.6% from the total

stripping charge. As Fig. V.8 illustrates, during CO oxidation a single rather broad peak was observed for Pt/GR-BDDP (curve 2), whereas at Pt/GR the same process leads to the occurrence of three intermingled peaks, which are usually ascribed to the presence of several types of active sites on which carbon monoxide species are differently bound.[264,265]

Nevertheless, on a relative basis, at Pt/GR carbon monoxide desorption appears to be facilitated to a certain extent since, as the integration of the stripping charges in Fig. V.8 revealed, ca. 23% of the CO is oxidized at potential values lower than that corresponding to the onset of the same process at Pt/GR-BDDP. There are reasons to believe that this could be the result of the higher amount of oxygenated Pt species (evidenced by XPS) that may act as oxygen donors, thus promoting CO oxidative desorption. Obviously, in our case this is only an apparent advantage because it was observed that at Pt/GR the overall CO desorption process is hindered by the particular morphology of the graphene substrate.

Anodic charges integrated during CO oxidation at both Pt/GR (curves 1a and 1b) and Pt/GR-BDDP (curve 2) allowed us to estimate active surface areas of the Pt deposits of ca. 19 $m^2 g^{-1}$ and ca. 17 $m^2 g^{-1}$ respectively, by assuming a value of 0.42 mC cm^{-2} for smooth platinum surface.[266] This was not unexpected since, as SEM measurements demonstrated, the use of a graphene support enables the deposition of smaller Pt particles. Nevertheless, the enhancement of the platinum specific surface area is less important than would have been expected based upon the rather large difference in size between particles deposited on the two substrates, observed with SEM. This indicates that for Pt/GR-BDDP the larger size of the Pt particles is compensated to some extent by the fact that, due to the morphology of the support, they are more accessible to the electrolyte solution.

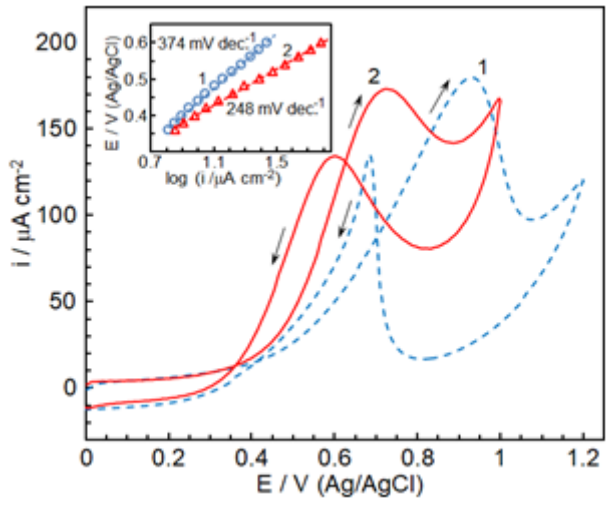

Fig. V.9 Cyclic voltammograms recorded during the fifth cycle in a 0.5 M H_2SO_4 +3.22 M CH_3OH solution (sweep rate, 20 mV/s) at Pt/GR (1) and Pt/GR-BDDP (2) electrodes. Inset: corresponding steady-state polarization results for methanol oxidation.

To gauge the effect of BDDP addition on the performances for methanol electrochemical oxidation of supported platinum, cyclic voltammetry experiments were performed and Fig. V.9 shows characteristic responses for Pt/GR (curve 1) and Pt/GR-BDDP (curve 2) recorded during the fifth consecutive run (sweep rate, 20 mV s^{-1}) in a 0.5 M H_2SO_4 + 3.22 M CH_3OH solution.

In both cases the shape of the voltammograms is typical of methanol oxidation at Pt electrodes in acidic media, exhibiting two well-defined anodic peaks: that one corresponding to methanol oxidation during the direct scan (peak potentials 0.928 V and 0.727 V for Pt/GR and Pt/GR-BDDP, respectively) and an additional peak on the reverse (cathodic) scan, located at lower

potential values, generally associated with the removal from the Pt surface of partially oxidized carbonaceous species formed during methanol oxidation.

For better comparison, the voltammetric current in Fig. V.9 was normalized to the electrochemically active surface area of the Pt catalyst as estimated above and it was observed that, although the height of the corresponding peaks recorded for the two types of electrodes are quite similar, the use of a GR-BDDP substrate results in a notable cathodic shift (ca. 200 mV) of the main oxidation peak. This behavior clearly indicates that the more loose structure of the support induced by the BDDP addition significantly facilitates the overall process. To gain better perspective on these findings steady-state polarization measurements were also carried out, in the same methanol-containing acidic solution, by increasing the applied potential in 20 mV steps and waiting 5 min after each step for the current to become relatively stable. The inset in Fig. V.9 illustrates the results, the Tafel plots yielding slopes of 374 mV decade^{-1} and 248 mV decade^{-1} for Pt/GR and Pt/GR-BDDP, respectively. One may observe, however, that by the use of the GR-BDDP substrate the slope for methanol oxidation is lowered with ca. 30% which is a non-negligible inherent advantage of the Pt/GR-BDDP system. It is worthy of note that, even without further optimization of the obtaining conditions, a Tafel slope of 248 mV decade^{-1} is still encouraging as it compares well with those reported in the literature for other electrode materials.

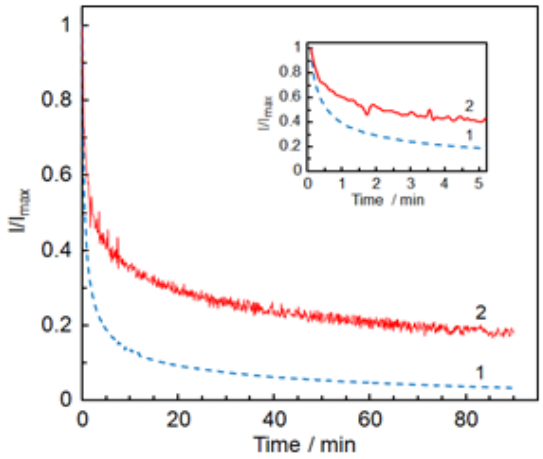

Fig. V.10 Time variation of the methanol oxidation current for Pt/GR (1) and Pt/GR-BDDP (2) in a 0.5 M H_2SO_4 + 3.22 M CH_3OH. Applied potential (V): 0.710 (1); 0.570 (2). Inset: corresponding chronoamperograms recorded during the early stage of the electrolysis.

The stability over time of the electrocatalytic activity of both types of electrodes was also investigated by chronoamperometry and Fig. V.10 illustrates the results of the long-term polarization measurements performed in the 0.5 M H_2SO_4 + 3.22 M CH_3OH solution. To ensure a reliable basis for comparison the experiments were carried out at applied potentials corresponding to those of the half-peaks (0.710 V and 0.570 V for Pt/GR and Pt/GR-BDDP, respectively) and the recorded methanol oxidation current was normalized to its maximum value (I/I_{max}). As the inset in Fig. V.10 shows, even during the early stage of the electrolysis the oxidation current decreases more sharply at Pt/GR electrodes and it was observed that after 90 min of continuous polarization its value reaches ca. 3.5% from the initial one, whereas at Pt/ GR-BDDP the decrease is less marked (down to ca. 18% from the maximum current). It seems reasonable to assume that this lower sensitivity to deactivation is the result of the fact that CO eviction from Pt sites is facilitated by the use of the GR-BDDP support, as demonstrated by the stripping experiments.

General conclusions

The present work addressed the possibility of using SiO_2 nanotubes, thin TiO_2 layers and conductive diamond-graphene composites as supports for platinum electrocatalysts. In all cases, before the development of the multicomponent electrode materials, the most straightforward methods were sought in order to render the three types of support suitable for being used as a substrate for the platinum electrocatalyst.

It was thus observed that the thermal treatment in a hydrogen atmosphere of theSiO_2 nanotubes results in an approximately four-fold increase in the surface concentration of defects (and therefore in a corresponding enhancement of the density of active centers) with obvious positive effects on the electrochemical activity.

The experiments aiming at using as a support thin TiO_2 films, spontaneously air-formed on the metallic titanium surface, demonstrated that a moderate laser treatment leads not only to an increase in the roughness (and therefore in the improvement of the electrochemically active surface area) but also to the disappearance of the surface titanium suboxides which could play the role of recombination centers. The lack of such centers enabled a better efficiency of the photogenerated charge carriers separation and therefore a more important degree of photoassistance.

In an attempt to improve the efficiency of the graphene layers as a support for electrocatalysts, moderate amounts of conductive diamond powder were embedded in them, a process that ensured both a better exposure of the more active edges planes of of the graphene structures, and an increased porosity of the layer resulting in an apparent electrocatalytic effect.

The investigated materials were used, both before and after the above specific treatments, as a support for the electrochemical deposition of platinum, the anodic oxidation of methanol being used as a test reaction to assess the electrocatalytic performances of the obtained multicomponent electrode materials. The electrochemical deposition of platinum is particularly advantageous because it ensures a good support-catalyst electrical contact and a more efficient use of the noble metal, since the entire amount deposited will be electrochemically active.

The results demonstrated that the investigated multicomponent materials show promising electrochemical and electrocatalytic properties, recommending them as possible replacements for classical Pt/C electrocatalysts in methanol fuel cells. For example, the use of the Pt/SiO_2-NT-H system allows methanol oxidation with Tafel slopes between 116 and 220 mV/decade, values comparable to those recorded for PtRu, $Pt\text{-}IrO_2$ or $Pt\text{-}Co_3O_4$ electrocatalysts. In terms of reliability and robustness, the replacement of the carbon support with one based on silicon oxide could lead, due to its special chemical and electrochemical stability, to a longer operating time and therefore to a more judicious use of the noble metal.

It was also observed that the laser treatment, to which the TiO_2 films were subjected before the platinum deposition, leads to a better electrocatalytic activity of the noble metal and to a better resistance to CO poisoning, as a combined effect of several

factors: a smaller size of the particles, a better Pt-TiO_2 electrical contact and an increased concentration of oxygen-containing surface groups, which can act as oxygen donors thus promoting the oxidative desorption of the reaction intermediates.

The use of Pt/GR-BDDP composites as electrode material for methanol oxidation led to encouraging results in terms of electrocatalytic activity and resistance to deactivation, most likely due to the fact that the higher porosity of the multicomponent material favors the access of active species from the solution.

Selected Bibliography

[94] N. Spataru, C. Anastasescu, M. M. Radu, I. Balint, C. Negrila,T. Spataru, A. Fujishima, The improvement of SiO_2 nanotubes electrochemical behavior by hydrogen atmosphere thermal treatment, **2018**, *Applied Surface Science*, Vol. 444, p.p. 216–223

[95] Xiao, L. Zhang, G. Meng, X. Tian, H. Zeng, M. Fang. High density aligned nanowire arrays: microscopic imaging of the unique growth style and their ultraviolet light emission properties, **2006**, *Journal of Physical Chemistry B*, Vol. 110, pp. 15724-15728.

[96] J. Wang, P.V.A. Pamidi, D.S. Park. Sol-gel-derived metal-dispersed carbon composite. Amperometric biosensors. **1997**, *Electroanalysis*, Vol. 9, pp. 52-55.

[97] F. Montilla, M. A. Cotarelo, E. Morallon. Hybrid sol-gel-conducting polymer synthesized by electrochemical insertion: tailoring the capacitance of polyaniline. **2009**, *Journal of Materials Chemistry*, Vol. 19, pp. 305-310.

[98] D. Salinas-Torres, F. Montilla, F. Huerta, E. Morallon.All electrochemical synthesis of polyaniline/silica sol-gel materials. **2011**, *Electrochimica Acta*, Vol. 56, pp. 3620-3625.

[99] A. Gamero-Quijano, F. Huerta, D. Salinas-Torres, E. Morallon, F. Montilla. Electrocatalytic performances of SiO_2-SWCNT nanocomposites prepared by electroassisted deposition. **2013**, *Electroanalysis*, Vol. 4, pp. 259-266.

[100] A. Gamero-Quijano, F. Huerta, D. Salinas-Torres, E. Morallon, F. Montilla. Enhancement of the electrochemical performance of SWCNT dispersed in a silica sol- gel matrix by reactive insertion of a conducting polymer. **2014**, *Electrochimica Acta*, Vol. 135, pp. 114-120.

[101] Y. Ren, H. Wei, X. Huang, J. Ding. Facile synthesis of SiO_2@C@graphene composites as anode material for lithium ion batteries. **2014**, *International Journal of Electrochemical Science*, Vol. 9, pp. 7784-7794.

[102] T. Spataru, T. Kondo, C. Anastasecu, I. Balint, P. Osiceanu, C. Munteanu, N. Spataru, A. Fujishima. Silica veils-conductive diamond powder composite as a new propitious substrate for platinum electrocatalysts. **2017**, *Journal of Solid State Electrochemistry*, Vol. 21, pp. 1007-1014.

[103] K. Gong, M. Zhang, Y. Yan, L. Su, L. Mao, S. Xiong, Y. Chen. Sol-gel derived ceramic-carbon nanotube nanocomposite electrodes: tunable electrode dimension and potential electrochemical applications. **2004**, *Analytical Chemistry*, Vol. 76, pp. 6500-6505.

[104] L. Skuja, Optically active oxygen-deficiency-related centers in amorphous silicon dioxide. **1998**, *Journal of Non-Crystalline Solids*, Vol. 239, pp. 16-48.

[105] S. S. Nekrashevich, V. A. Gritsenko, Electronic structure of silicon dioxide (a review), , **2014**, *Physics of the Solid State*, Vol. 56, pp. 207–222.

[106] F. Agullo-Lopez, A. Climent-Font, A. Munoz-Martin, J. Olivares, A. Zucchiatti, Ion beam modification of dielectric materials in the electronic excitation regime: cumulative and exciton model, **2016**, *Progress in Materials Science*, Vol. 76, pp. 1–58.
[107] V. Ryabchuk, Photophysical processes related to photoadsorption and photocatalysis on wide band gap solids: a review, **2004**, *International Journal* of Photoenergy, Vol. 6, pp.95–113.
[108] Y. G. Andreev, P. G. Bruce, Demonstrating structural deformation in an inorganic nanotube, **2008**, *Journal of the American Chemical Society*, Vol. 130, pp. 9931–9934.
[109] C. Anastasescu, M. Zaharescu, D. Angelescu, C. Munteanu, V. Bratan, T. Spataru, C. Negrila, N. Spataru, I. Balint, Defect-related light absorption, photoluminescence and photocatalytic activity of SiO_2 with tubular morphology, **2017**, *Solar Energy Materials & Solar Cells*, Vol. C 159, pp. 325–335.
[114] N. Spataru, K. Tokuhiro, C. Terashima, I. Sutanto, D. A. Tryk, S. M. Park, A. Fujishima, Electrochemical behavior of cobalt oxide films deposited at conductive diamond electrodes, **2003**, *Journal of the Electrochemical Society*, Vol. 150, pp. E337–E341.
[115] N. Spataru, X. T. Zhang, T. Spataru, D. A. Tryk, A. Fujishima, Anodic deposition of RuO_x_nH_2O at conductive diamond films and conductive diamond powder for electrochemical capacitors, **2008**, *Journal of the Electrochemical Society*, Vol. 155, pp. D73–D77.
[116] T. Spataru, M. Marcu, N. Spataru, Electrocatalytic and photocatalytic activity of Pt-TiO_2 films on boron-doped diamond substrate, **2013**, *Applied Surface Science*, Vol. 269, pp. 171–174.
[117] Y. S. Chaudhary, J. Ghatak, U. M. Bhatta, D. Khushalani, One-step method for self-assembly of metal nanoparticles onto facetted hollow silica tubes, **2006**, *Journal of Materials Chemistry*, Vol. 16, pp. 3619–3623.
[118] D. Wang, Y. Li, Z. Lin, B. Qiu, L. Guo, Surface-enhanced electrochemiluminescence of Ru@SiO_2 for ultrasensitive detection of carcinoembryonic antigen, **2015**, *Analytical Chemistry*, Vol. 87, pp. 5966-5972,
[119] J. Goldberger, R. Fan, P. Yang, Inorganic nanotubes: a novel platform for nanofluids. **2006**, *Accounts of Chemical Research*, Vol. 39, pp. 239-248.
[126] H. Yoshida, Silica-based quantum photocatalysis for selective reactions. **2003**, *Solid State and Materials Science*, Vol. 7, pp. 435-442.
[127] L. Yuliati, T. Hattori, H. Yoshida, Highly dispersed magnesium oxide species on silica as photoactive sites for photoinduced direct methane coupling and photoluminescence, **2005**, *Physical Chemistry Chemical Physics*, Vol. 7, pp. 195-201.
[128] F. J. Grunthaner, P. J. Grunthaner, R. P. Vasquez, B. F. Lewis, J. Mesergian, Local atomic and electronic structure of oxide/GaAs and SiO_2/Si interfaces using high-resolution XPS, **1979**, *Journal of Vacuum Science and Technology*, Vol. 16, pp. 1443-1453.
[129] A. Thogersen, J. H. Selj, E. S. Marstein, Oxidation effects on graded porous silicon anti-reflection coatings, D, **2012**, *Journal of the Electrochemical Society*, Vol. 159, pp. 276-281.
[130] Y. Ikuta, K. Kajihara, M. Hirano, Sh. Kikugawa, H. Hosono, Effects of H_2 impregnation on excimer-laser-induced oxygen-deficient center formation in synthetic SiO_2 glass, **2002**, *Applied Physics Letters*, Vol. 80, pp. 3916-3918.

[138] X. Lu, J. Hu, J. S. Foord, Q. Wang, Electrochemical deposition of Pt-Ru on diamond electrodes for the electrooxidation of methanol, **2011**, *Journal of Electroanalytical Chemistry*, Vol. 654, pp. 38-43.
[139] G. Wu, L. Li, B. Q. Xu, Effect of electrochemical polarization of PtRu/C catalysts on methanol electrooxidation, **1999**, *Electrochimica Acta*, Vol. 50, pp. 1-10.
[140] X. Lu, J. Hu, J. S. Foord, Q. Wang, Electrochemical deposition of Pt-Ru on diamond electrodes for the electrooxidation of methanol, **2011**, *Journal of Electroanalytical Chemistry*, Vol. 654, pp. 38-43.
[141] T. J. Schmidt, H. A. Gasteiger, R. J. Behm, Methanol electrooxidation on a colloidal PtRu-alloy fuel-cell catalyst, **1999**, *Electrochemistry Communications*, Vol. 1, pp. 1-4.
[142] C. Roth, N. Martz, F. Hahn, J. M. Leger, C. Lamy, H. Fuess, Characterization of differently synthesized Pt-Ru fuel cell catalysts by cyclic voltammetry, FTIR spectroscopy and single cells. E, **2002**, *Journal of the Electrochemical Society*, Vol. 149, pp. 433-439.
[146] M. M. Radu, N. Becherescu, T. Spataru, P. Osiceanu, M. A. Mihai, J. M. Calderon-Moreno, N. Spataru, A. Fujishima, Improved suitability as catalyst support and more efficient charge carrier separation of native air-formed TiO_2 films by mild laser treatment, **2019**, *Journal of Power Sources*, 437, 226921
[147] K. Kordesch, G. Simander, Fuel Cells and Their Applications, **1996**.
[148] H. A. Gasteiger, J. Garche, In Handbook of Heterogeneous Catalysis, **2008**, p. 3084.
[149] N. Spataru, X. Zhang, T. Spataru, D. A. Tryk, A. Fujishima, Platinum, electrodeposition on conductive diamond powder and its application to methanol oxidation in acid media, B, **2008**, *Journal of the Electrochemical Society*, Vol. 155, pp. 264-269.
[161] J. V. Macpherson, J. P. Gueneau de Mussy, J. L. Delplancke, High-resolution electrochemical, electrical, and structural characterization of a dimensionally stable $Ti/TiO_2/Pt$ electrode, B, **2002**, *Journal of the Electrochemical Society*, Vol. 149, pp. 306-313.
[190] J. W. Schultze, M. M. Lohrengel, Stability, reactivity and breakdown of passive films. Problems of recent and future research, **2000**, *Electrochimica Acta*, Vol. 45, pp. 2499-2513.
[191] S. Proch, S. Yoshino, N. Takahashi, S. Kosaka, K. Kodama, Y. Morimoto, CO-terminated Pt/Au codeposition on titania nanotube arrays (TNAs), **2017**, *Electrocatalysis*, Vol. 8, pp. 480-491.
[192] S. Proch, S. Yoshino, N. Takahashi, J. Seki, S. Kosaka, K. Kodama, Y. Morimoto, The native oxide on titanium metal as a conductive model substrate for oxygen reduction reaction studies, **2018**, *Electrocatalysis*, Vol. 9, pp. 608-622.
[193] S. Trasatti, Electrocatalysis in the anodic evolution of oxygen and chlorine, **1984**, *Electrochimica Acta*, Vol. 29, pp. 1503-1512.
[194] A. D. Battisti, G. Lodi, M. Cappadonia, G. Battaglin, R. Kotz, Influence of the valve metal oxide on the properties of ruthenium based mixed oxide electrodes: II. RuO_2/TiO_2 coatings, **1989**, *Journal of the Electrochemical Society*, Vol. 136, pp. 2596-2598.
[195] K. W. Kim, E. H. Lee, J. S. Kim, K. H. Shin, K. H. Kim, Effect of an etching Ti substrate on a catalytic oxide electrode, B, **2001**, *Journal of the Electrochemical Society*, Vol. 148, pp. 111-115.
[196] T. Prikhna, A. P. Shapovalov, G. E. Grechnev, V. G. Boutko, A. A. Gusev, A. V. Kozyrev, M. A. Belogolovskiy, V. E. Moshchil, V. B. Sverdun, Formation of nanostructure

in magnesium diboride based materials with high superconducting characteristics, **2016**, *Low Temperature Physics*, Vol. 42, pp. 380-394.
[197] A. V. Naumkin, A. Kraut-Vass, S. W. Gaarenstroom, C. J. Powell, NIST X-ray photoelectron spectroscopy database. NIST standard reference database 20, **2012**.
[202] J. N. Tiwari, R. N. Tiwari, G. Singh, K. S. Kim, Recent progress in the development of anode and cathode catalysts for direct methanol fuel cells, **2013**, *Nano Energy*, Vol. 2, pp. 553-578.
[203] J. J. Pietron, M. B. Pomfret, C. N. Chervin, J. W. Long, D. R. Rolison, Direct methanol oxidation at low overpotentials using Pt nanoparticles electrodeposited at ultrathin conductive RuO2 nanoskins, **2012**, *Journal of Materials Chemistry*, Vol. 22, pp. 5197-5204.
[204] G. Q. Lu, W. Chrzanowski, A. Wieckowski, Catalytic methanol decomposition pathways on a platinum electrode, B, **2000**, *Journal of Physical Chemistry*, Vol. 104, pp. 5566-5572.
[205] T. Iwasita, Electrocatalysis of methanol oxidation, **2002**, *Electrochimica Acta*, Vol. 47, pp. 3663-3674.
[206] C. S. Chen, F. M. Pan, Electrocatalytic activity of Pt nanoparticles deposited on porous TiO_2 supports toward methanol oxidation, **2009**, *Applied Catalysis B: Environmental*, Vol. 91, pp. 663-669.
[207] K. Fukutani, M. B. Song, Y. Murata, Photodesorption of CO and CO^+ from Pt(111): mechanism and site specificity, **1995**, *Journal of Physical Chemistry*, Vol. 103, pp. 2221-2228.
[216] N. Spătaru, J. M. Calderon-Moreno, P. Osiceanu, T. Kondo, C. Terashima, M. Popa, M. M. Radu, D. Culiţă, L. Preda, M. A. Mihai, T. Spătaru, Conductive diamond powder inclusion in drop-casted graphene for enhanced effectiveness as electrocatalyst substrate, **2020**, *Chemical Engineering Journal*, 402, 126258
[217] R. L. McCreery, Advanced carbon electrode materials for molecular electrochemistry, **2008**, *Chemical Reviews*, Vol. 108, pp. 2646-2687.
[228] H. J. Choi, S. M. Jung, J. M. Seo, D. W. Chang, L. Dai, J. B. Baek, Graphene for energy conversion and storage in fuel cells and supercapacitors, **2012**, *Nano Energy*, Vol. 1, pp. 534-551.
[229] D. A. C. Brownson, L. J. Munro, D. K. Kampouris, C. E. Banks, Electrochemistry of graphene: not such a beneficial material, **2011**, *RSC Advances*, Vol. 1, pp. 978-988.
[230] C. E. Banks, T. J. Davies, G. G. Wildgoose, R. G. Compton, Electrocatalysis at graphite and carbon nanotube modified electrodes: edge-plane sites and tube ends are the reactive sites, **2005**, *Chemical Communications*, Vol. 36, pp. 829-841.
[241] J. Yan, T. Wei, B. Shao, F. Ma, Z. Fan, M. Zhang, C. Zheng, Y. Shang, W. Qian, F. Wei, Electrochemical properties of graphene nanosheet/carbon black composites as electrodes for supercapacitors, **2010**, *Carbon*, Vol. 48, pp. 1731-1737.
[242] L. Qiu, X. Yang, X. Gou, W. Yang, Z.F. Ma, G. G. Wallace, D. Li, Dispersing carbon nanotubes with graphene oxide in water and synergistic effects between graphene derivatives, **2010**, *Chemistry—A European Journal*, Vol. 16, pp. 10653- 10658.
[243] A. Fujishima, Y. Einaga, T. N. Rao, D. A. Tryk (ed.), Diamond Electrochemistry. BKC Inc., Tokyo, **2005**.

[244] L. Cunci, C. R. Cabrera, Preparation and electrochemistry of boron-doped diamond nanoparticles on glassy carbon electrodes, **2011**, *Electrochemical and Solid- State Letters*, Vol. 14, pp. 17-19.
[245] S. Nantaphol, R. B. Channon, T. Kondo, W. Siangproh, O. Chailapakul, C. S. Henry, Boron-doped diamond paste electrodes for microfluidic paper-based analytical devices, **2017**, *Analytical Chemistry*, Vol. 89, pp. 4100-4107.
[256] Y. Xin, J. Guo Liu, Y. Zhou, W. Liu, J. Gao, Y. Xie, Y. Yin, Z. Zou, Preparation and characterization of Pt supported on graphene with enhanced electrocatalytic activity in fuel cell, **2011**, *Journal of Power Sources*, Vol. 196, pp. 1012-1018.
[257] K. Panda, B. Sundaravel, B. K. Panigrahi, P. Magudapathy, D. Nandagopala Krishna, K. G. M. Nair, H. C. Chen, I. N. Lin, Structural and electronic properties of nitrogen ion implanted ultra nanocrystalline diamond surfaces, **2011**, *Journal of Applied Physics*, Vol. 110, pp. 044304-1-9.
[258] M. Marcu, T. Spataru, J. M. Calderon-Moreno, P. Osiceanu, L. Preda, N. Spataru, Anodic voltammetry of epinephrine at graphene-modified conductive diamond electrodes and its analytical application, B, **2018**, *Journal of the Electrochemical Society*, Vol. 165, pp. 523-529.
[266] T. Vidakovic, M. Christov, K. Sundmacher, The use of CO stripping for in situ fuel cell catalyst characterization, **2007**, *Electrochimica Acta*, Vol. 52, pp. 5606- 5613.

DISSEMINATION OF RESULTS

Papers published in ISI-listed scientific journals whose results were the subject of the doctoral thesis:

1. Nicolae Spătaru, Crina Anastasescu, **Mihai Marian Radu**, Ioan Balint, Catalin Negrila, Tanța Spătaru, Akira Fujishima, The improvement of SiO_2 nanotubes electrochemical behavior by hydrogen atmosphere thermal treatment, 2018, *Applied Surface Science*, Vol. 444, p.p. 216–223 **(IF: 5.155)**

2. Mihai Marian Radu, Nicu Becherescu, Tanța Spăataru, Petre Osiceanu, Marius Alexandru Mihai, Jose Maria Calderon-Moreno, Nicolae Spătaru, Akira Fujishima, Improved suitability as catalyst support and more efficient charge carrier separation of native air-formed TiO_2 films by mild laser treatment, 2019, *Journal of Power Sources*, Vol. 437, Nr. 226921 **(IF: 8.247)**

3. Nicolae Spătaru, Jose Maria Calderon-Moreno, Petre Osiceanu, Takeshi Kondo,Chiaki Terashima, Monica Popa, **Mihai Marian Radu**, Daniela Culiță, Loredana Preda,Marius Alexandru Mihai, Tanţa Spătaru, Conductive diamond powder inclusion in drop-casted graphene for enhanced effectiveness as electrocatalyst substrate,2020, *Chemical Engineering Journal*, Vol. 402, Nr. 126258
(IF: 13.273)

Works published in ISI-listed scientific journals that are related to the topic of the PhD thesis (results not included in the PhD thesis):

1. Rodica Daniela Baratoiu, Marioara Bem, Ana Cristina Radutiu, Tanta Spataru, **Mihai Marian Radu**, Mariana Voicescu, Gabriela Ionita, Nicolae Stanica, Titus Constantinescu, Alexandru T. Balaban, 1-Picryl-2-phenyl-2-(4-picrylamidophenyl) diazenium betaine and its radical-anion: synthesis and physical properties, 2017, *Monatsh Chem*,Vol.148, p.p.1411–1416 **(IF: 1.285)**

2. Loredana Preda, Takeshi Kondo, Tanta Spataru, Mariana Marin, **Mihai Marian Radu**, Petre Osiceanu, Akira Fujishima, Nicolae Spataru, Enhanced Activity for Methanol Oxidation of Platinum Particles Supported on Iridium Oxide Modified Boron-Doped Diamond Powder, 2017, *ChemElectroChem*, Vol.4, Nr. 8, p.p. 1908-1915 **(IF: 4.446)**

3. Tanța Spătaru, **Mihai Marian Radu**, Nicolae Spătaru, Akira Fujishima, Voltammetric determination of N-hydroxysuccinimide at conductive diamond electrodes, 2018, *Analyst*, Vol.10 **(IF: 4.019)**

4. Cristina Maria Buta, **Mihai Marian Radu**, Alice Mischie, Christina Marie Zălaru, Gabriela Ioniță, Marilena Ferbinteanu, Experimental and computational characterization of structural and spectroscopic features of mixed ligand copper complexes-prototypes for square-pyramidal stereochemistry, 2019, *Polyhedron*, Vol. 170, p.p. 771–782 **(IF: 2.343)**

5. Tanța Spătaru, Marius Alexandru Mihai, Loredana Preda, Maria Marcu, **Mihai Marian Radu**, Nicolae Dan Becherescu, Alin Velea, Mohamed Yassine Zaki, Radu Udrea , Veronica Satulu, Nicolae Spătaru, Enhanced photoelectrochemical activity of WO_3-decorated native titania films by mild laser treatment, 2022, *Applied Surface Science*, Vol. 596, Nr.153682 **(IF: 7.392)**